Chapter 1

Laves Phase in Alloy 718 Fusion Zone

S.G.K. Manikandan, D. Sivakumar and M. Kamaraj

Additional information is available at the end of the chapter

http://dx.doi.org/10.5772/intechopen.70325

Abstract

The gas tungsten arc (GTA) welded fusion zone of alloy 718 has been well investigated on the formation of interdendritic Laves phase. This article deals with the various process control methodologies for minimizing the microsegregation and Laves phase such as the enhanced weld cooling rate in GTA welding (GTAW) process and modification in weld metal chemistry. Even though the high energy density welding processes such as electron beam (EB) and laser beam (LB) welding techniques are proven in minimizing the microsegregation and Laves phase, the requirement of conventional GTA welding process still exists in the aerospace industry due to the complex shapes of the components and the inaccessible conditions for executing the welding process. The enhancement in the weld cooling rate and modified weld metal chemistry resulted in the refined fusion zone microstructure and reduced microsegregation. Enhanced weld efficiency on ultimate tensile strength (UTS) and 0.2% YS at 25°C was observed to the tune of 85 to 93% by employing cryogenic cooling in GTA welding process. Similar improvement in weld efficiency at 650°C was observed. However, the evaluated weld efficiencies with cryogenically cooled weld metal were marginally lower than the previous works in EB and LB welds only by 2–3%.

Keywords: Laves phase, alloy 718, GTAW, X-ray diffraction, tensile strength, microsegregation

1. Introduction

Alloy 718 is extensively used in the high-temperature systems of cryogenic rocket engines in Indian launch vehicles. Use of Nb as age hardener in place of Al or Ti in alloy 718 eliminated the problem of strain age cracking, but resulted in the formation of brittle interconnected Laves phase during welding [1] which are the favorable sites for easy crack

initiation and propagation. This affects the aging response, tensile properties, and ductility of the welded components [2]. Hence control on the morphology and continuity of the Laves phase during solidification was found to be essential. Published information on the control of Laves phase formation in alloy 718 welds is limited to autogenous welds of gas tungsten arc welding (GTAW), electron beam welding (EBW) and laser beam welding (LBW) [3], current pulsing with simple square waveform and magnetic arc oscillation in GTAW [4]. It was concluded that the faster cooling rate reduced the level of interdendritic Nb segregation and amount of Laves phase. But high energy density processes cannot be adopted in rocket engines due to the complex shapes and highly inaccessible areas. Zhang and Liu reported that the cooling rate was enhanced with the higher growth rate and steep temperature gradient [5]. Hence pulse current manual GTA welding process is relied upon with limited options such as modified pulse waveform [6] and helium shielding gas to enhance the cooling rate and minimize the segregation. Their effect on formation of Laves phase and microsegregation of niobium in alloy 718 fusion zone has been discussed.

The influence of cryogenic coolants on microstructures was investigated earlier [6, 7]. Hence rapid heat dissipation dynamics using liquid nitrogen was studied in the present work during manual GTA welding process for further enhancing the weld cooling rate. Filler metals with significantly different compositions from that of the base material composition were used to minimize Laves phase in some of the welding applications [8]. This was the driving force for studying the solidification behavior of alloy 718 fusion zone welded with high Mo (16 wt%) filler metal, even though it was well established by various researchers [9, 10]. The present study also describes the influence of hybrid pulsing in the range of 500–2000 Hz on the fusion zone microstructure and interdendritic segregation of alloy 718 welds. The effects of pulse frequency have been analyzed through solidification parameters and related mechanisms on the interdendritic segregation in alloy 718 fusion zone. In view of the above, an attempt has been made in the present study to evaluate the effectiveness of cooling techniques in controlling the formation of Laves phase and the high-temperature mechanical properties in alloy 718 GTA welds.

Primarily, this chapter deals with the control of laves phase formation in the fusion zones of alloy 718 weldments by enhanced weld cooling rate through modified pulse current waveform and shielding gases (Argon and Helium) in GTA welding process and change of weld metal chemistry using solid solution (FM1) and matching composition/age-hardenable (FM2) filler metal. Secondly, the mechanical properties at room temperature and elevated temperatures have been correlated to the Laves phase in the weld fusion zone of alloy 718.

2. Materials and methods

The specimens were prepared from alloy 718 sheets of 2 mm thick (for welding experiments) and 3 mm (for solidification experiments) in 980°C solution treated condition using gas tungsten arc welding process. The solidification experiments were conducted in autogenous mode GTAW with thermocouples welded at the center of the weld and adjacent to the fusion zone in a 5 × 5 array in order to obtain both longitudinal and transverse temperature distribution. The details of the chemical composition for base material and filler metal are given in **Table 1**. The weld

Element	C	Mn	Si	Cr	Fe	Mo	Nb + Ta	Ti	Al	Cu	Ni
Base metal	0.05	0.11	0.1	18.2	19.8	2.8	5	1	0.6	0.03	Bal.
FM1	0.05	2	0.5	16	5	16	-	-	-	-	Bal.
FM2	0.08	0.55	0.4	21	16	3.3	5.5	1.15	0.8	0.3	Bal.

Table 1. Chemical composition of base metal and filler metals (in wt%).

parameters for square butt joints with an optimized heat input value of 0.75–0.77 kJ/mm were employed. The conventional copper heat sink and liquid nitrogen were used for the external cooling. Similarly, modified pulse wave form (constant current, compound current, and hybrid pulsing) with argon and helium shielding gas were employed for the in-process cooling.

Welded samples were subjected to the aging treatment as per AMS 5596 K after 100% X-ray radiography and dye penetrant test. The samples were etched using Kalling's reagent and the weld microstructures and elemental mapping were obtained with field emission gun scanning electron microscope (FE-SEM) with an acceleration voltage of 20 kV. The elemental mapping of Nb in the dendritic and interdendritic zones was carried out in a thermal field emission electron microprobe (EPM JXA-8530F) over the metallographically prepared and unetched specimens with an acceleration voltage of 15 kV.

Electron diffraction studies were carried out with 3 mm diameter and 90 μm thickness discs of the as-welded and the direct-aged fusion zone using Jeol make transmission electron microscope (TEM) equipment. Differential thermal analysis was conducted to finalize the heating rate among the three heating rates of 5, 10, and 20°C/min using SII 6300 EXSTAR with a sample weight of 0.02 ± 0.0005 g in an argon atmosphere at a flow rate of 0.2 l/min. Differential scanning calorimetric analysis was performed on a SETARAM LABSYS 1600 heat flux type DSC instrument to measure eutectic type reaction temperatures with an optimized heating rate of 10°C/min and a cooling rate of 20°C/min. The tensile test of the specimen at 25 and 650°C were conducted at a strain rate of 1×10^{-3} s^{-1} as per ASTM E8 and E21-09, respectively. An air circulating furnace with accuracy in temperature of ±3°C was used for conducting the 650°C tensile test. The fracture morphology was studied using scanning electron microscope.

3. Microstructural characterization of fusion zone

The conventionally cooled GTA welded fusion zone microstructure using argon shielded constant current technique (weld cooling rate: 40°C/s) revealed a mixed dendritic structure consisting of columnar and/or elongated dendritic and equiaxed dendritic structures as shown in **Figure 1(a)**. The fusion zone exhibited coarse columnar dendrites from the fusion line to the middle of the fusion zone due to the experimentally measured longitudinal temperature gradient in the order of −39.26°C/mm along the welding direction.

But the fusion zone of compound current pulse with conventional cooling measured a weld cooling rate of 394°C/s, the corresponding fusion zone exhibited a finer equiaxed dendritic structure as shown in **Figure 1(c)**. The transition from columnar-to-equiaxed (CET) was

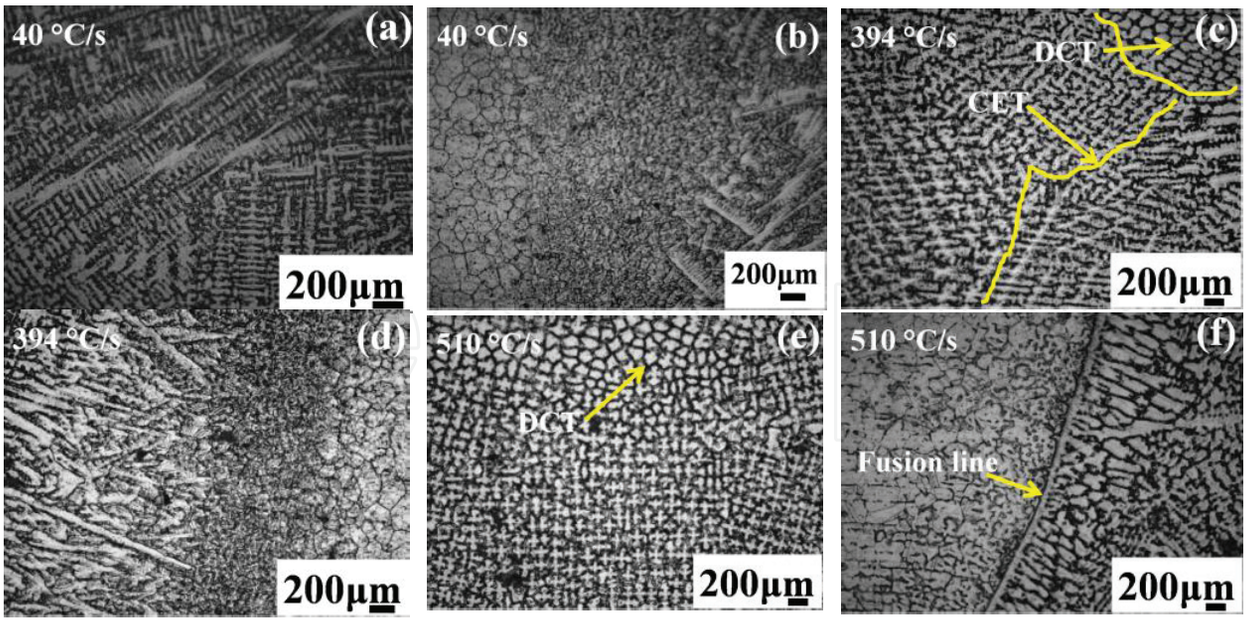

Figure 1. Micrographs of conventionally cooled fusion zones (a, c), heat affected zones (b, d) and cryogenically cooled fusion zone (e), heat affected zone (f) using constant current (40°C/s) and compound current pulse technique (394, 510°C/s), respectively.

shifted away from the center of the fusion zone by the enhanced longitudinal temperature gradient existed ahead of the columnar front of the order of −195.16°C/mm. The base material grains were recrystallized and epitaxial growth was initiated with finer grains which led to the formation of fine columnar dendritic structure near to the heat affected zone as evidenced in **Figure 1(d)**.

Similar observations were made on the microstructures of the cryogenically cooled (liquid nitrogen) GTA welded fusion zone with finer equiaxed dendritic structures than that of the conventional cooling method as shown in **Figure 1(e)** for the same set of welding variables (as used for the weld cooling rate of 394°C/s). The refinement of fusion zone microstructure was due to the imposed cooling rate. The extent of refinement of the fusion zone microstructure was also enhanced till the middle of the fusion zone. Certain regions in the middle of the fusion zone revealed the dendrite to cellular transition as shown in **Figure 1(e)** by the degeneration of side branches through dendrite arm remelting mechanism due to the variation in the morphology parameter (temperature gradient/growth rate—G/R). As presented in **Figures 1(b)**, **(d)**, and (f), and **2(e)** and **(f)**, microfissures were not observed in the heat affected zone of both the conventionally cooled and liquid nitrogen-cooled weldments. The base material grains were coarsened in the lowest weld cooling rate (40°C/s). The grain growth was limited with the enhanced cooling rate as shown in **Figure 2(f)**, especially in the liquid nitrogen-cooled weldments through the reduced transverse temperature gradient by the impingement of cold nitrogen vapor.

The SE micrographs of conventionally cooled fusion zone exhibited a thick and continuous interdendritic Laves network as shown in **Figure 2(a)** due to the increased time at temperature parameter and reduced longitudinal temperature gradient (−39.26°C/mm) which led to a

http://dx.doi.org/10.5772/intechopen.70325

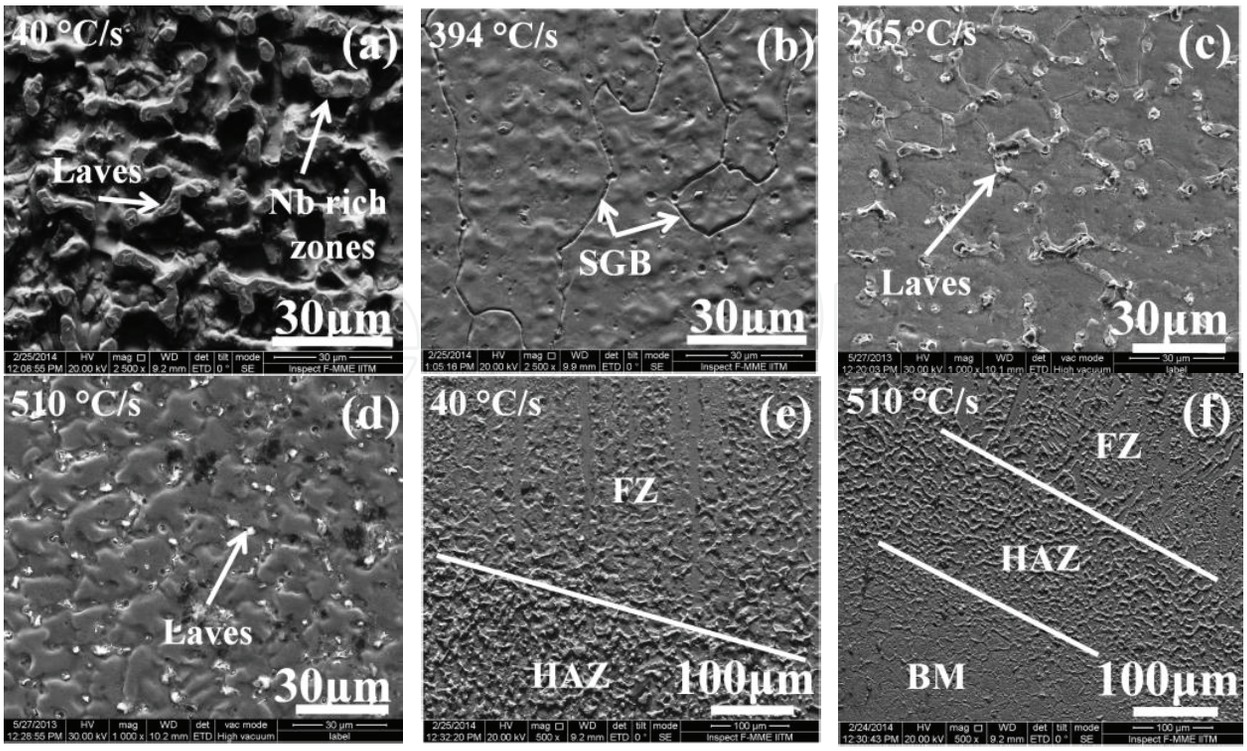

Figure 2. SE micrographs of (a, b) conventionally cooled, (c, d) liquid nitrogen-cooled GTA welded fusion zone and (e, f) respective heat affected zone.

lower weld cooling rate (40°C/s) and higher solidification time resulted an enhanced microsegregation. **Figure 3** details about the quantitative elemental analyses of GTA weld fusion zone for the six weld cooling rates (40, 80, 394, 265, 362, and 510°C/s).

The quantitative elemental analysis exhibited that microsegregation was reduced with increased weld cooling rate. This was revealed by the increase of niobium content in the dendritic regions of both the FM1 and FM2 fusion zone with the weld cooling rate. As shown in **Figure 2(a)**, the Nb rich zones present in the FM2 fusion zone (40°C/s) exhibited relatively higher niobium content in the dendritic region due to the pickup from the adjacent zones. As the iron content increased in the dendrite, more of niobium was rejected into the interdendritic regions due to the limited solubility of Nb which resulted in the increased microsegregation [8]. The fusion zone (394°C/s) microstructure consisted of γ-matrix with clear solidification grain boundaries and discrete Laves particles in the interdendritic regions as in **Figure 2(b)**.

The microsegregation was significantly reduced by employing the in-process cooling method such as compound current pulse and helium shielding gas which enhanced the longitudinal temperature gradient and growth rate. Thus the fusion zone microstructure was refined. The liquid nitrogen-cooled fusion zone microstructures for the constant current (265°C/s) mode revealed finer and disconnected interdendritic Laves particles as shown in **Figure 2(c)**. As the weld cooling rate was increased to 510°C/s by employing the compound current pulse mode, the microstructure of the fusion zone was further refined and resulted with relatively finer Laves particles as shown in **Figure 2(d)**. Since the interdendritic microsegregation was

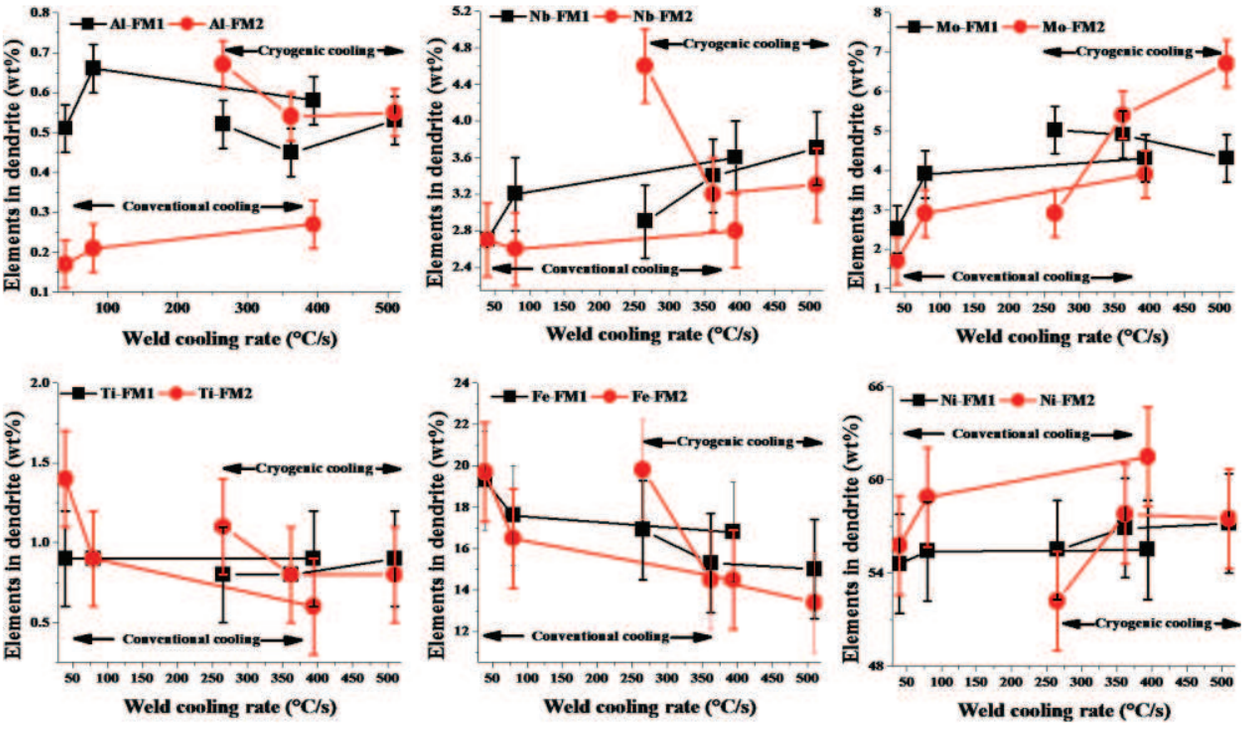

Figure 3. Elemental analysis of alloy 718 fusion zone using FE-SEM/EDS.

reduced, the dendrite was enriched with niobium for the higher weld cooling rates. It was observed that Nb concentration in FM2 fusion zone was comparable to the base material composition at higher weld cooling rate (510°C/s). As the iron content was decreasing (k_{Fe} =0.98 to 0.76 for FM1 and k_{Fe} = 1 to 0.63 for FM2) with the increase in weld cooling rate as given in **Figure 3** which aided in reducing the microsegregation. In addition, an increase in nickel content at higher weld cooling rate (510°C/s) was observed. This helped in retaining the Nb content in the matrix and thereby the concentration of Nb in the dendritic regions was increased.

As discussed previously, the decrease of iron content in the dendrite core with the increased weld cooling rate indicated that the weld dilution levels were reduced for the maximum cooling rate employed in the present study. The present study took advantage of the modified pulse waveform and the helium shielding gas which aided in constricting the arc; thereby, the weld dilution levels were minimized in the present study. Hence the solubility of niobium and molybdenum were increased because of the reduced iron content in γ matrix and the resultant interdendritic segregation was also reduced. In our present study, the distribution trend of elements in the fusion zone was comparable with the previous research work [8]. However, the localized niobium rich zones in FM2 fusion zone modified the elemental distribution trend of niobium at lowest weld cooling rate. The HAZ of both the weldments were free from microfissures and grain boundary liquation as shown in **Figure 2(e)** and **(f)** due to the balanced transverse temperature gradient because of the longitudinal holes on the top of the cooling system with an angle of attack for cooling the HAZ region. The interdendritic phases in the fusion zone were found to be of C14 type Laves phases with hcp crystal structure (a = 0.4831 nm, c = 0.7881 nm) as shown in **Figure 4(a)**. The matrix was found to be

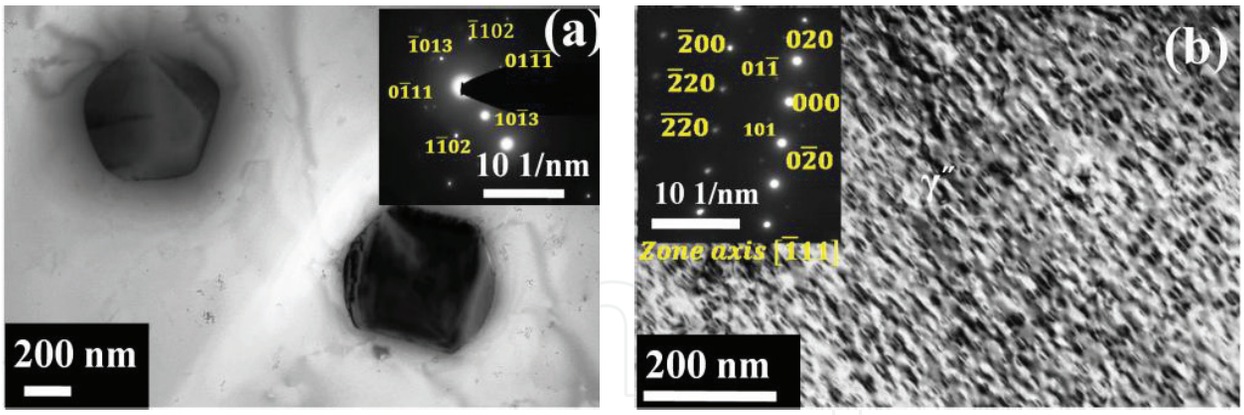

Figure 4. TEM bright field image with SADP pattern of (a) Laves phase in as-welded fusion zone, TEM dark field micrograph of direct-aged fusion zone (b) γ″ precipitates with zone axis [−1 1 1].

polycrystalline in nature with face centered cubic crystal structure (a = 0.3571 nm) for the fusion zone of higher weld cooling rates (394°C/s and above).

The aging response was also confirmed by the TEM dark field images. The respective selected area diffraction pattern is shown in **Figure 4(b)**. Disc-shaped γ″ precipitates and spherical γ′ precipitates were observed. The Laves phase morphology and its crystal structure were not affected by the imposed thermal gradient and enhanced weld cooling rate. The script type morphology of the Laves particles was retained for the employed weld cooling rates.

The partition ratio of the individual elements was calculated from the FE-SEM/EDS data using dendrite microsegregation model. The partition coefficient of niobium in the FM1 fusion zone was increased from 0.54 to 0.72 in the conventionally cooled fusion zone. This could be due to the decrease in iron and chromium contents (**Figure 3**). However, the partition ratio of niobium (0.54–0.97) in the FM2 fusion zone was found to be more than that of the FM1 fusion zone. The fusion zones of lower weld cooling rates exhibited higher Laves phases because of the huge segregation of niobium and molybdenum (k_{Nb} = 0.54) toward liquid. Obviously, a steep concentration gradient was built in the interdendritic liquid by the lower diffusivity and/or mobility parameter of molybdenum through solutal undercooling. This led to a better refinement in microstructure. The BSE micrograph of the liquid nitrogen-cooled FM2 fusion zone revealed the reduced interdendritic segregation as shown in **Figure 5(a)**. The elemental mapping also confirmed the reduced microsegregation of niobium as shown in **Figure 5(b)**. The finer distribution of Laves particles aided in improving the mechanical properties of the liquid nitrogen cooled weldment. However, the characteristic temperatures in DSC analysis were not affected significantly for the liquid nitrogen-cooled FM1 fusion zone from that of the conventionally cooled alloy 718 fusion zone.

In the present study, liquidus temperature (primary γ) of the FM1 fusion zone was not significantly changing from that of the base material for the lower weld cooling rates of 40–362°C/s. But a significant increase in liquidus temperature was observed with the higher employed cooling rates of 394 and 5107°C/s due to the enhanced molybdenum content in the matrix at these cooling rates as shown in **Figure 3**. The partitioning of higher melting point solute (Mo) to γ matrix led to the increase in the solvus temperature of γ matrix. Whereas the liquidus

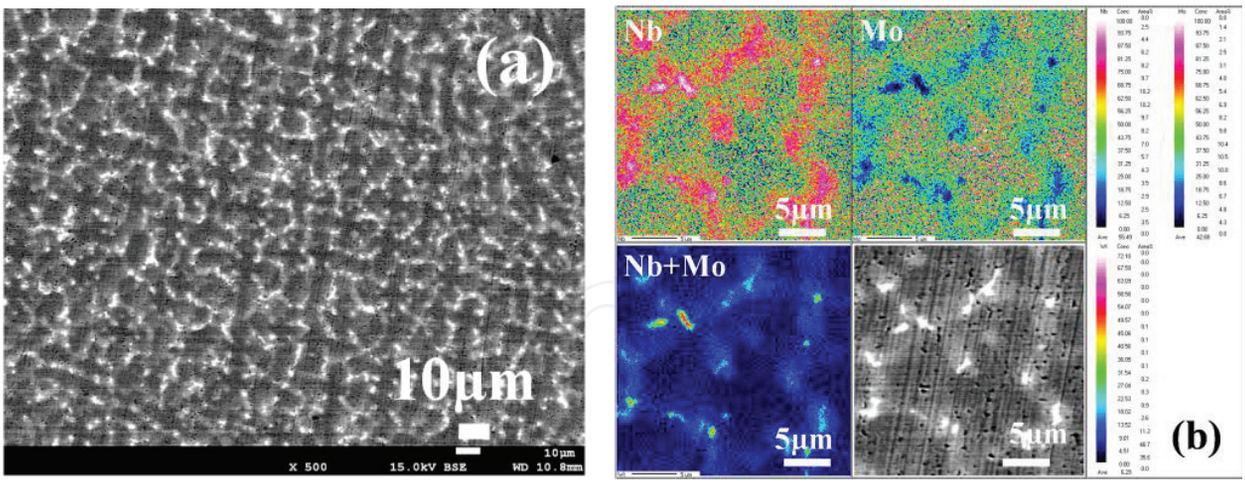

Figure 5. BSE image of FM2 fusion zone for a weld cooling rate of (a) 510°C/s and (b) elemental mapping in EPMA.

temperature of FM2 fusion zone was decreasing as the cooling rate was increased due to the increased solute concentration in the matrix as per the phase diagram, at higher cooling rates, the liquidus temperature of FM2 fusion was comparable to that of the base material. The solidification time for each employed weld cooling rate was calculated using heat transfer experiments and DSC analysis and found reduced from 2.099 to 0.12 s for the enhanced weld cooling rate from 40 to 394°C/s. This was further reduced to 0.011 s for the liquid nitrogen cooling method. The SE micrographs of the fusion zones of hybrid pulsing using argon and helium shielding gases are shown in **Figure 6(a)–(f)**. In the present study, the modified

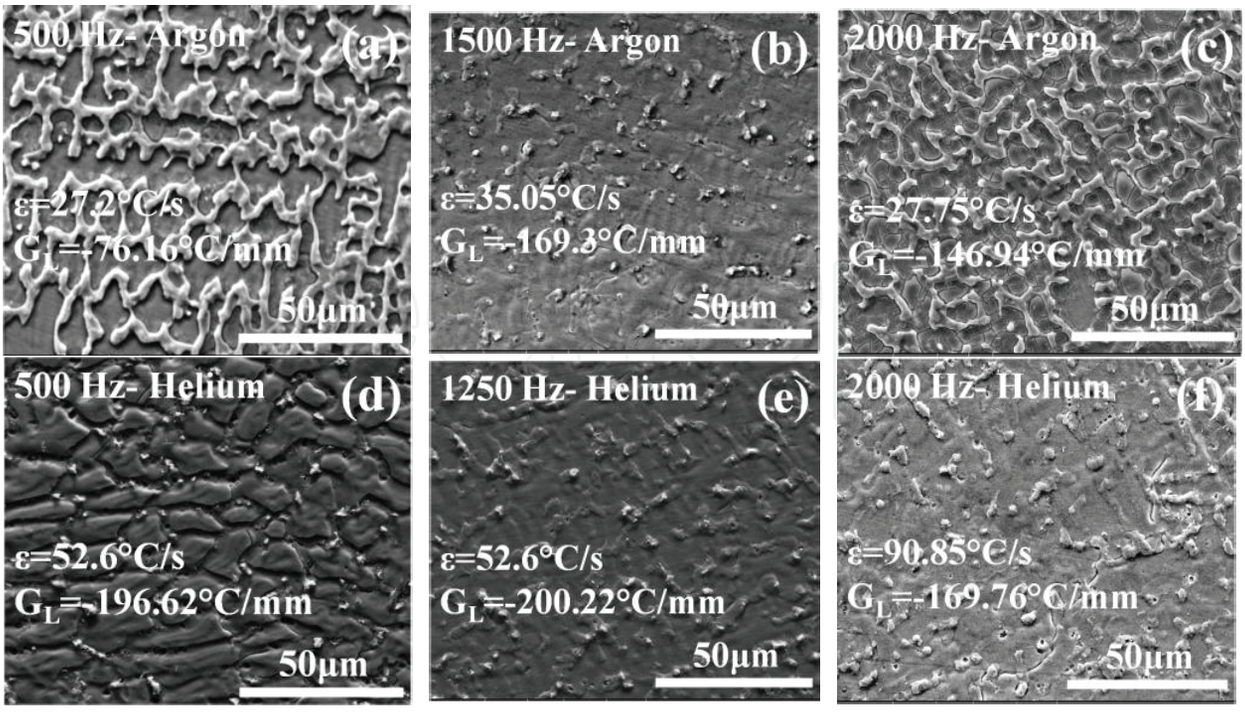

Figure 6. SE micrographs of (a–c) argon and (d–f) helium shielded as-welded fusion zone using hybrid pulse current.

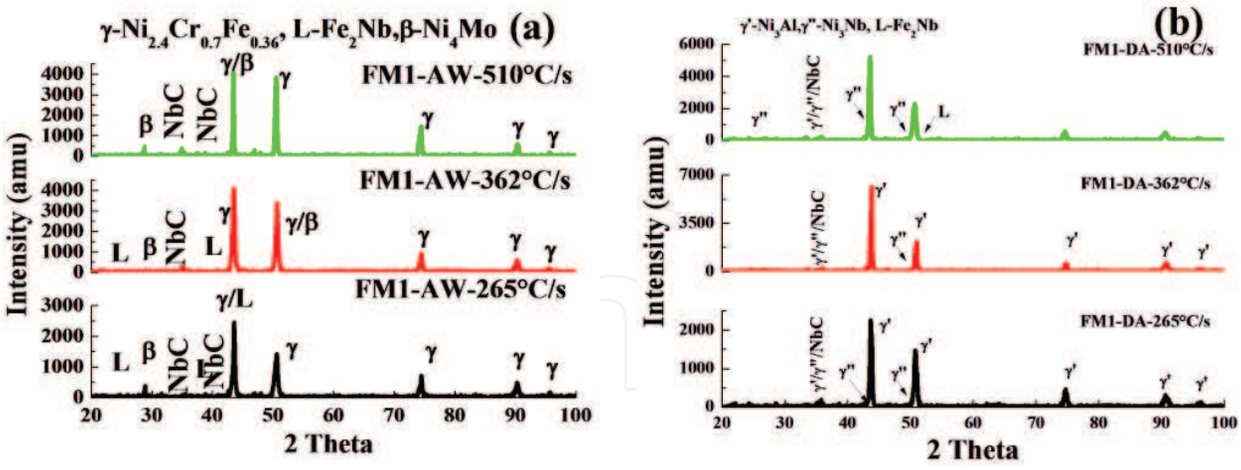

Figure 7. X-ray diffraction patterns of the fusion zone of three different weld cooling rates with FM1 in (a) as-welded and (b) direct-aged conditions.

pulsing increased plasma momentum and electro-magnetic force inside the weld pool and led to the refined microstructure. Thus, the interdendritic Laves phase was reduced.

The fluctuation in radiation had been reduced in the pulse frequency range of 500–2000 Hz and therefore the heat transfer efficiency of the arc was improved. The increased plasma momentum enhanced the arc pressure. In addition, the lower pulse ratio was resulted by the subdivision of peak pulse time with superimposed high frequency pulsing. The combination of the above phenomenon was giving rise to the convective flow. This aided in the equiaxed growth ahead of columnar growth. However, the fluctuations induced by the pulsing current alone were not aiding the fragmentation of dendrites in mushy zone. The solute enrichment at the dendrite root caused the dendrite remelting. Hence, the finer secondary dendritic arms were fractured and/or fragmented easily and further aided by the stirring action and/or by viscous friction caused by the relative movement between liquid and solid metal.

The phases formed in the fusion zone were analyzed using the representative X-ray diffractograms as shown in **Figure 7(a)** and **(b)**. The diffraction peaks indicated the presence of γ matrix, MC type carbides, and Laves phase in the as-welded condition for both the FM1 and FM2 fusion zones. The lattice parameter of γ matrix was calculated using Nelson-Riley method and found an increased lattice constant (0.36113 nm) for FM1 fusion zone due to the increased solute (Mo) content in the dendrite. In addition, FM1 fusion zone exhibited β-Ni4Mo phase in the as-welded condition and got dissolved after direct aging treatment as shown in **Figure 7(a)** and **(b)**. The direct-aged specimens of fusion zone showed the diffraction peaks of γ″/γ′ precipitates, MC type carbides, and Laves phase.

4. Mechanical property characterization of weldments

The hardness distribution in the weld metal was executed through microhardness survey. The experimental conditions are as follows:

- Condition: As welded, Duration: 15 s, Load: 2.942 N.
- Condition: Direct aged, Duration: 15 s, Load: 9.807 N.

The microhardness survey on the welded samples is given in **Table 2**. As inferred from the microhardness survey, the liquid nitrogen cooling method produced softer weldments than that of the conventionally cooling method.

The increased microsegregation and the existence of Laves phases led to the increased hardness in the as-welded condition for the conventionally cooled weld metal. The upper limit of the hardness values for the as-welded and direct-aged conditions mentioned in **Table 2** was corresponding to the lower and higher weld cooling rates, respectively. Moreover, the liquid nitrogen-cooled FM1 (solid solution filler metal) fusion zone well responded for the direct aging process as the fusion zone hardness values were comparable with FM2 (age hardenable filler metal) fusion zone. The results of room temperature (25°C) and high-temperature (650°C) tensile tests conducted on the welded specimen with six levels of weld cooling rate are given in **Figure 8(a)** and **(b)** for the conventional and liquid nitrogen cooling methods.

The room temperature tensile test data revealed that the weld strength properties in direct-aged condition were improved with CCP technique than that of the previous works on the same alloy system [1, 3]. The room temperature ultimate tensile strength (UTS) of the conventionally cooled weldment increased with the enhanced weld cooling rate for both the FM1 (987–1105 MPa) and FM2 (1256–1284 MPa).

The UTS values of conventionally cooled FM1 fusion zone was less than that of the FM2 fusion zone after direct aging at both 25 and 650°C. However, the tensile strength of welds was improved for the weldments cooled with liquid nitrogen. The high-temperature strength values were increased with the enhanced weld cooling rate. The UTS of liquid nitrogen-cooled FM1 fusion zone (1038 MPa) was higher than that of the FM2 fusion zone (1005 MPa) for the same weld cooling rate (510°C/s). This could be due to the reduced grain growth by the retention of molybdenum in the dendrite [11]. The microstructures were refined in FM1

Cooling method	Filler metal	Hardness of fusion zone (Hv)	
		As welded	Direct aged
Conventional	FM1	205–365	363–418
	FM2	238–406	410–454
Liquid nitrogen cooling	FM1	221–269	310–475
	FM2	204–237	309–475
Hybrid pulsing	FM1-Argon	250–375	350–415
	FM1-Helium	260–380	375–418
	FM2-Argon	230–250	330–440
	FM2-Helium	210–280	350–438

Table 2. Hardness of fusion zone.

http://dx.doi.org/10.5772/intechopen.70325

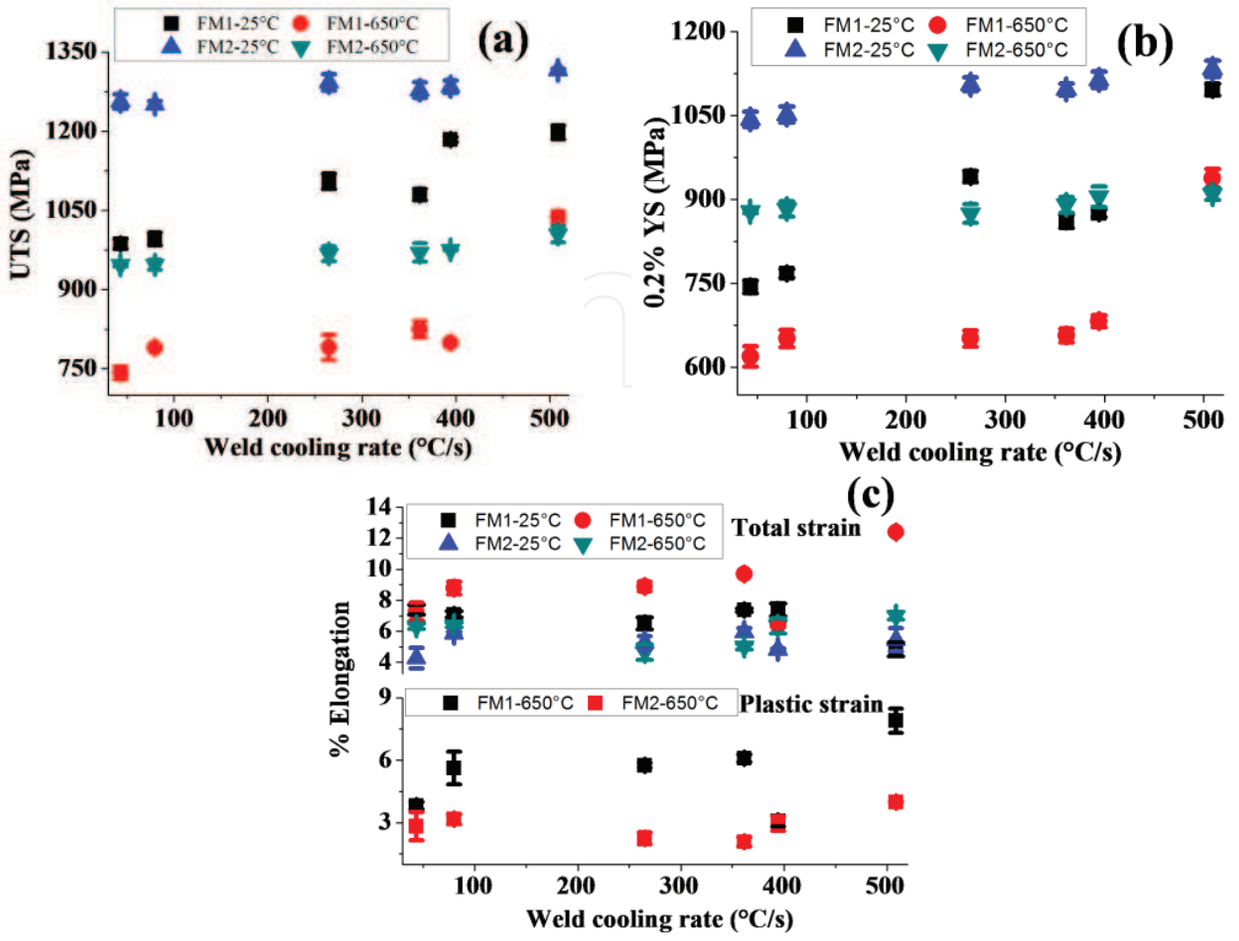

Figure 8. Tensile properties [(a, b) tensile strength and (c) strain] of conventionally and cryogenically cooled FM1 and FM2 weldments at 25 and 650°C.

fusion zone due to the addition of molybdenum which promoted solutal undercooling by the concentration gradient. Hence, the combined effect of thermal and solutal undercooling resulted in a refined microstructure.

The fracture surfaces of the room temperature tensile specimens at 25°C for DA conditions revealed the equiaxed dimple morphology. The fracture surface investigation in SEM indicated a detrimental nature of the Laves phase in fracture process even at 650°C. The fractographs of 650°C tensile tested specimen of FM1 and FM2 are as shown in **Figure 9(a)** and **(b)** for the conventional cooling process.

Among the six fusion zones of different weld cooling rates, the FM1 fusion zone exhibited deep dimple features at 650°C. The fractured surfaces of 650°C testing exhibited a mixed mode (inter and transgranular modes) of fracture with a unique dendritic pattern. The fracture was progressed along the Laves phase. The Laves particles were observed inside the dimple surface for the fusion zones of 40°C/s as shown in **Figure 9(b)**. The microcracks were initiated preferentially by decohesion of laves phase–γ matrix interface under the action of a tensile stress and resulted in a premature failure. The wedge type cracking features were observed in both FM1 and FM2 fusion zones.

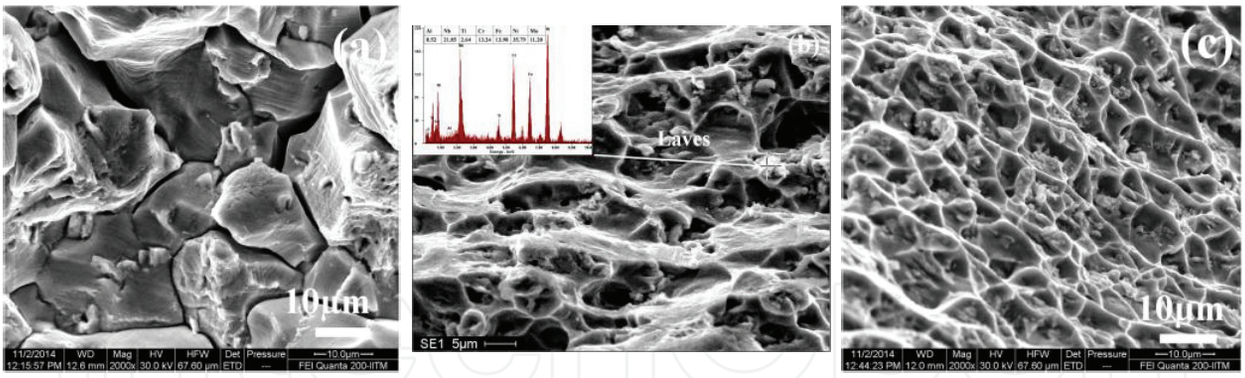

Figure 9. Fractographs of (a, b) conventionally cooled and (c) liquid nitrogen-cooled fusion zones tensile tested at 650°C.

The fractographs of the liquid nitrogen-cooled weldments exhibited transgranular fracture as shown in **Figure 9(c)**. It was proved that the tensile properties of the alloy 718 weldment were reduced at room temperature conditions, especially the weld ductility. Similar results were obtained at room temperature in the present study. In addition, it was observed in the present work that at 650°C tensile properties were also reduced as the Laves particles favored crack initiation and continuous Laves network aided the crack propagation. This led to the easier fracture process. The fracture process was progressed by the nucleation of voids and subsequent growth of macroscopic cracks along the weaker laves-matrix interface even at 650°C. Thus, weld ductility was reduced. As the Laves network was disrupted and refined, equiaxed dendritic microstructure associated with fine and discrete Laves particles enhanced the tensile properties both at 25 and 650°C. The plastic strain of the cryogenically cooled weld metal was higher than that of the conventionally cooled weld metal as shown in **Figure 8(c)**. The liquid nitrogen-cooled fusion zone had increased molybdenum content in the dendrite (4–5 wt%) and molybdenum-bearing phase was observed in the XRD analysis of FM1 fusion zone as shown in **Figure 7(a)**. These phases pinned the grain boundaries and enhanced the plastic strain in liquid nitrogen-cooled weldments.

The room temperature mechanical properties of the hybrid pulsing weldments were evaluated and the maximum tensile strength of 1155 and 1100 MPa for argon and helium shielded FM1 fusion zones at 500 and 2000 Hz, respectively. Similarly, maximum tensile strengths were obtained at 2000 Hz in the argon and helium shielded FM2 (1330 MPa) fusion zones. The maximum yield strength (965 MPa) was obtained in the intermediate pulse frequency (1250 Hz) for the argon shielded FM1 fusion zone and (856 MPa) at 2000 Hz in the helium shielded fusion zone. FM2 fusion zone exhibited a maximum of 1138 MPa yield strength for both argon and helium shielded fusion zone at 1500 and 2000 Hz, respectively. The maximum weld ductility was demonstrated for the helium shielded FM1 weldments than that of the other hybrid pulsing weldments. The high-temperature tensile testing of the transverse welded specimens revealed an ultimate tensile strength values ranging from 989.53 to 1030.15 MPa (±16.79 MPa) and 0.2% yield strength values from a minimum of 843.33 MPa to a maximum of 885 MPa (±17.68 MPa). The ductility of the weld was lower in the range of 3.48–3.6% (±0.14) and a plastic strain of 1–1.26% (±0.05%).

http://dx.doi.org/10.5772/intechopen.70325

5. Inferences

The interdendritic Laves phase formation during GTA welding of alloy 718 has been investigated using enhanced weld cooling rates and change of weld metal chemistry. The volume fraction of Laves phase was reduced from 45.95 to 8% with the enhanced weld cooling rate by the combination of modified pulse current and helium shielding gas for both FM1 and FM2 fusion zones. This was further reduced to 0.1% while employing cryogenic cooling during GTA welding process. The high energy density processes minimized Laves phase and prone for HAZ microfissures. GTA welding process employed with liquid nitrogen cooling aided in minimizing laves phase and free of HAZ microfissures. Enhanced weld efficiency on UTS and 0.2% YS at 25°C was observed to the tune of 85–93% by employing cryogenic cooling in GTA welding process. Similar improvement in weld efficiency at 650°C was observed. However, the evaluated weld efficiencies with cryogenically cooled weld metal were marginally lower than the previous works in EB and LB welds only by 2–3%. Moreover, it was observed that the Laves network influenced the strength of the weldment at 650°C. The modification of weld metal chemistry with Mo solute element through solid solution filler metal (FM1) promoted solutal undercooling, in addition to the thermal undercooling. Thus, the microstructures were refined and Laves phase formation was reduced. The intermediate pulse frequencies were aiding better Laves phase control for the argon shielded GTA welding process and the same results were obtained with 2000 Hz pulse frequency in the helium shielded process. This could be due to the combined effect of longitudinal temperature gradient while using different shielding gases and shape factor of the pulse wave form.

Author details

S.G.K. Manikandan[1]*, D. Sivakumar[1] and M. Kamaraj[2]

*Address all correspondence to: nehakutty06@gmail.com

1 Indian Space Research Organisation, India

2 Indian Institute of Technology Madras, India

References

[1] Mills WJ. Effect of microstructural variations on the tensile and fracture toughness properties of Inconel 718 weldments. In: Loria PA, editor. Proc. Conf. on 718 alloy. PA: TMS; 1984. pp. 845-858

[2] Reddy GM, Murthy CVS, Srinivasa Rao K, Prasad RK. Mint: Improvement of mechanical properties of Inconel 718 electron beam welds—influence of welding techniquesand postweld heat treatment. International Journal of Advanced Manufacturing Technology. 2009;**43**:671-680

[3] Ram GDJ. Effect of Laves phase on mechanical properties on Inconel 718 welds [Thesis]. Chennai: IIT Madras, Department of Metallurgical and Materials Engineering; 2004

[4] Sivaprasad K, Ganesh Sundararaman S. Mint: Influence of weld cooling rate on microstructure and mechanical properties of alloy 718 weldments. Metallurgical and Materials Transactions A. 2008;**39**(9):2115-2127

[5] Zhang W, Liu L. Mint: Solidification microstructure of directionally solidified superalloy under high thermal gradient. Rare Metals. 2012;**31**(6):541-546

[6] Wang J, Kusumoto K, Nezu K. Mint: Analysis of electrical characteristics for hybrid pulsed micro-tungsten inert gas welding arc. Science and Technology of Welding and Joining. 2004;**9**(4):369-373

[7] Amuda MOH, Mridha S. Mint: Grain refinement and hardness distribution in cryogenically cooled ferritic stainless steel welds. Materials Design. 2013;**47**:365-371

[8] Banovic SW, Du Pont JN, Marder AR. Mint: Dilution and microsegregation in dissimilar metal welds between super austenitic stainless steel and nickel base alloys. Science and Technology of Welding and Joining. 2002;**7**(6):374-383

[9] Knorovsky GA, Cieslak MJ, Headley TJ, Romig Jr. AD, Hammetter WF. Mint: Inconel 718: A solidification diagram. Metallurgical and Materials Transactions A. 1989; **20**(10):2149-2158

[10] Du Pont JN, Robino CV, Micheal JR, Notis MR, Marder AR. Mint: Solidification of Nb-bearing superalloys: Part I. Reaction sequences. Metallurgical and Materials Transactions A. 1998;**29A**:2785-2796

[11] Han D, Liu F, Jia D, Qi F, Yang H, Sun W, Hu Z. Effect of Mo addition on the grain growth of IN718 alloy. Materials Science Forum. 2015;**816**:594-600